Quark cluster model for deep-inelastic lepton-deuteron scattering

G. Yen, J. P. Vary, and A. Harindranath
Physics Department, Iowa State University, Ames, Iowa 50011
and Physics Department, The Ohio State University, Columbus, Ohio 43210

H. J. Pirner
Institut für Theoretische Physik, Universität Heidelberg, D-6900 Heidelberg, Federal Republic of Germany
(Received 18 June 1990)

We evaluate the contribution of quasifree nucleon knockout and of inelastic lepton-nucleon scattering in inclusive electron-deuteron reactions at large momentum transfer. We examine the degree of quantitative agreement with deuteron wave functions from the Reid soft-core and Bonn realistic nucleon-nucleon interactions. For the range of data available there is strong sensitivity to the tensor correlations which are distinctively different in these two deuteron models. At this stage of the analyses the Reid soft-core wave function provides a reasonable description of the data while the Bonn wave function does not. We then include a six-quark cluster component whose relative contribution is based on an overlap criterion and obtain a good description of all the data with both interactions. The critical separation at which overlap occurs (formation of six-quark clusters) is taken to be 1.0 fm and the six-quark cluster probability is 4.7% for Reid and 5.4% for Bonn. As a consequence the quark cluster model with either Reid or Bonn wave function describe the SLAC inclusive electron-deuteron scattering data equally well. We then show how additional data would be decisive in resolving which model is ultimately more correct.

I. INTRODUCTION

Deep-inelastic lepton-nucleus inclusive reactions (abbreviated DIS) have been the subject of much discussion recently.[1] As the momentum transfer of the probe increases we expect the degrees of freedom relevant for the description of the process to change from hadrons to quarks. At what range of momentum transfer this transition takes place is, at present, a matter of controversy. In order to elucidate the role of non-nucleonic degrees of freedom and possible exotic phenomena in high-energy lepton-nucleus interactions one must first evaluate the contribution of nucleonic degrees of freedom within conventional models including quasielastic and inelastic processes. The main purpose of this work is to assemble existing results and present new results that support the following claims.

(1) For all the available deep-inelastic lepton-deuteron inclusive data for $Q^2 \geq 1$ GeV^2 and Bjorken $x > 0.5$ there is a substantial contribution from quasielastic nucleon knockout evaluated from conventional nuclear models in lowest order and from Fermi motion smearing of the nucleon inelastic structure function.

(2) Comparisons between the Reid soft-core[2] (RSC) and Bonn[3] wave-function results for DIS on deuterium (nucleon quasielastic and inelastic processes only) display substantial sensitivity to tensor correlations in the range of existing data. Within this approach the stronger tensor forces of RSC provide a better but not satisfactory agreement with these data.

(3) Including the six-quark cluster effects of the quark cluster model[4] (QCM) provides a good description of all these DIS on deuterium data with both interactions.

This paper is organized as follows. In Sec. II we review the model used for the calculation of quasielastic nucleon knockout, the chief features of the chosen deuterium wave functions, and introduce the choice of the nucleon form factors. In Sec. III we summarize the model for smearing the nucleons' inelastic structure functions to obtain the "three-quark (3-q) cluster" contribution to the deuterium inelastic structure function. We combine the quasielastic contribution and the 3-q inelastic structure function in Sec. IV and compare with SLAC data.[5-7] In Sec. V we introduce the "six-quark (6-q) cluster" contribution of the QCM. Finally Sec. VI contains the results from the full QCM and Sec. VII contains our conclusions.

II. MODEL FOR INCLUSIVE (e,e') REACTION NEAR THE QUASIELASTIC PEAK

We begin this section by establishing our notation for lepton-nucleus scattering. We then introduce the model for the quasifree nucleon knockout process which assumes that we know only the ground-state nucleon three-momentum distribution in the target rest frame and that we can neglect the final-state interactions. This model could be used with either a relativistic or nonrelativistic dynamical picture of the nucleus which yields this ground-state distribution. This treatment represents a smearing over the Fermi motion which is approximate and open for discussion. Eventually it would be desirable to have a fully consistent treatment of the hadronic dynamics and kinematics, but this is not presently available to our knowledge. This is especially challenging, since, to

be realistic for our purposes, such a consistent model must reproduce the nucleon-nucleon (N-N) scattering data and the deuterium ground-state properties.

The electron scattering cross section from a free nucleon or from a free nucleus in the laboratory frame when no spin information is retained is usually written as

$$\frac{d^2\sigma}{d\Omega\, dE'} = \sigma_M \left[W_2(|\mathbf{q}|,\nu) - 2W_1(|\mathbf{q}|,\nu)\tan^2\frac{\theta}{2} \right] , \tag{1}$$

where the Mott cross section σ_M is given by

$$\sigma_M = \frac{\alpha^2}{4E^2}\frac{\cos^2(\theta/2)}{\sin^4(\theta/2)} . \tag{2}$$

Here θ is the lepton scattering angle, E the incident energy and E' the outgoing energy of the electron, $\mathbf{q}$ is the three-momentum transfer, ν is the energy transfer with the quantities expressed in the laboratory system, and α is the fine structure constant. The square of the four-momentum transfer is $q^2=\nu^2-|\mathbf{q}|^2=-Q^2$. The structure functions W_1 and W_2 appear in the response tensor $W^{\mu\nu}$ which may be written as

$$\begin{aligned} W^{\mu\nu} &= \tilde{g}^{\mu\nu}W_1 + \tilde{P}^{\mu}\tilde{P}^{\nu}W_2 \\ &= (2\pi)^6 \sum_{P_x} \langle P_x|J_\nu^N(0)|P\rangle^* \\ &\quad \times \langle P_x|J_\mu^N(0)|P\rangle \delta^4(P+q-P_x) , \end{aligned} \tag{3}$$

with

$$\tilde{g}^{\mu\nu} = g^{\mu\nu} - \frac{q^\mu q^\nu}{q^2} , \tag{4}$$

and

$$\tilde{P}^{\mu} = \left[P^\mu - \frac{(P\cdot q)q^\mu}{q^2} \right] \frac{1}{M_T} . \tag{5}$$

$|P\rangle$ denotes the target state and M_T is the mass of the target. The interpretation of the sum over the states $|P_x\rangle$ is as follows: In the case of elastic scattering from an isolated nucleon there is only a plane-wave state $|P_x\rangle$ consistent with four-momentum conservation; in the case of quasifree nucleon knockout from an isolated nucleus initially at rest, the states $|P_x\rangle$ consist of a continuum nucleon of momentum $\mathbf{k}$ and a residual nucleus of momentum $-\mathbf{k}$. The longitudinal and transverse response functions are given by

$$R_L(|\mathbf{q}|,\nu) = \frac{|\mathbf{q}|^2}{q^2}\left[-W_1(|\mathbf{q}|,\nu) + \frac{|\mathbf{q}|^2}{q^2}W_2(|\mathbf{q}|,\nu) \right] , \tag{6}$$

$$R_T(|\mathbf{q}|,\nu) = -2W_1(|\mathbf{q}|,\nu) . \tag{7}$$

The most frequently employed model for quasifree nucleon knockout is based on a nonrelativistic Schrödinger picture of the nucleus. For very light nuclei exact numerical ground-state wave functions have been obtained for realistic N-N interactions. Consequently, these wave functions feature high momentum components in the single nucleon motion which arise from tensor and short-range correlations. Below, we examine the deuteron case in detail to elucidate these features.

Consider elastic lepton-nucleon scattering from a nucleon moving in the laboratory frame with a three-momentum $\mathbf{k}$ and energy $E_1(|\mathbf{k}|)$. In keeping with the usual impulse approximation, the neglect of final-state interactions and the neglect of the flux factor, and $E_1(|\mathbf{k}|)$ fixed by the conservation of energy and momentum with an on-shell spectator nucleus we arrive at

$$\begin{aligned} \frac{d^2\sigma}{d\Omega\, dE'} &= \sigma_M \frac{m^2\delta(\nu+E_1(|\mathbf{k}|)-E(|\mathbf{k}+\mathbf{q}|))}{E(|\mathbf{k}+\mathbf{q}|)E_1(|\mathbf{k}|)} \\ &\quad \times \left[W_2^{\rm el} - 2W_1^{\rm el}\tan^2\frac{\theta}{2} \right] , \end{aligned} \tag{8}$$

where

$$W_2^{\rm el} = F_1^2 + \frac{\kappa^2 Q^2}{4m^2}F_2^2 , \tag{9}$$

$$W_1^{\rm el} = -\frac{Q^2}{4m^2}(F_1+\kappa F_2)^2 . \tag{10}$$

Here F_1 and F_2 are the Dirac and Pauli form factors and κ is the anomalous magnetic moment. The nucleon mass is denoted by m. The spinors have been normalized such that $\bar{u}u=1$. We are following the conventions of Bjorken and Drell.[8]

The above result holds for a neutron or a proton and has been obtained with an average over the nucleon spin. To finish embedding this in a nucleus in our simplest approximation scheme we assume that the nucleon has a laboratory momentum distribution $n(|\mathbf{k}|)\equiv n(k)$ in the initial state given by any dynamical model and we average over this initial state:

$$\begin{aligned} \frac{d^2\sigma}{d\Omega\, dE'} &= (Z\sigma_p + N\sigma_n) \\ &\quad \times \int d^3k\, n(k) \frac{m\delta(\nu+E_1(|\mathbf{k}|)-E(|\mathbf{k}+\mathbf{q}|))}{E(|\mathbf{k}+\mathbf{q}|)} , \end{aligned} \tag{11}$$

with

$$\sigma_j = \sigma_M \left[W_2^{(j)} - 2W_1^{(j)}\tan^2\frac{\theta}{2} \right] , \tag{12}$$

where j stands for n or p, and

$$\int d^3k\, n(k) = 1 . \tag{13}$$

It is important to note that a factor $m/E_1(|\mathbf{k}|)$ has been absorbed into $n(k)$ by virtue of the normalization chosen. We utilize the symmetry and the delta function to reduce the cross section to a single dimensional integral. This results in

$$\frac{d^2\sigma}{d\Omega\, dE'} = (Z\sigma_p + N\sigma_n)\frac{2\pi m}{|\mathbf{q}|}\int_{k_l}^{k_u} n(k)k\, dk , \tag{14}$$

with

$$k_u = a+b ,$$

$$k_l = |a-b| ,$$

with

$$a=\frac{\nu+M_T}{2}\left[\left[1-\frac{(M^*_{A-1}+m)^2}{\Lambda^2}\right]\times\left[1-\frac{(M^*_{A-1}-m)^2}{\Lambda^2}\right]\right]^{1/2}, \quad (15)$$

$$b=\frac{|\mathbf{q}|}{2}\left[1+\frac{(M^*_{A-1})^2-m^2}{\Lambda^2}\right], \quad (16)$$

where

$$\Lambda^2=(\nu+M_T)^2-|\mathbf{q}|^2, \quad (17)$$

$$M^*_{A-1}=M_T-m+\epsilon, \quad (18)$$

$$\epsilon=\epsilon_B+\epsilon^*. \quad (19)$$

In the above ϵ_B is the energy to remove a single nucleon and leave the $A-1$ system in the ground state and ϵ^* is any excitation energy in the residual system. In this application to deuterium $M_T=M_d$, $M^*_{A-1}=m$, and $\epsilon^*=0$.

For sufficiently large $|\mathbf{q}|$ the integral in Eq. (14) becomes approximately a function of only k_l. It comes as no surprise that k_l is the same as the "y" variable chosen by some authors[9] in analyzing data and other models. It is worth noting again that the result for $d^2\sigma/d\Omega\,dE'$ holds within our approximation for relativistic and nonrelativistic models for $n(k)$ when appropriately normalized. In particular one does not obtain factors such as $d\nu/dk_{\|}$ or $d\nu/dy$ which often appear in place of $m/|\mathbf{q}|$ in some authors' expression for $d^2\sigma/d\Omega\,dE'$.

The approximations in obtaining this model involve the neglect of a convection current contribution[10] and the use of on-shell form factors. We have examined this convection current contribution in the context of an extreme single-particle shell model of the nucleus and found it to be small when $Q^2\gtrsim 0.25$ GeV^2. We have used on-shell form factors since to our knowledge there is no unique theory for off-shell nucleon form factors.[11]

To treat the Fermi motion effects at the level of evaluating a theory of the scattering amplitude (as opposed to smearing a cross section in our model above), we adapted the relativistic formalism of Ref. 10 (Celenza *et al.*) to a calculation using nonrelativistic wave functions. In this treatment we confirmed the convection current contribution was negligible. In this calculation, as everywhere else, we employed on-shell form factors. For $Q^2\gtrsim 0.25$ GeV^2 the results of this calculation were indistinguishable from the results obtained using the model presented in this work.

We concentrate on deuterium, which is not only the simplest of nuclei with the lowest binding energy per particle and the lowest average density, but is also the nucleus for which the DIS (e,e') data are available over the widest kinematic range. The primary focus here is on the intermediate momentum components of two deuteron wave functions which are constrained to reproduce the measured low-energy properties of deuterium. Since the system is so weakly bound and so diffuse it is also the system for which our approximation of neglecting final-state interactions should be more accurate.

In Fig. 1 we present the single nucleon momentum distributions in the deuteron $n(k)$ emerging from the ground-state wave functions of the RSC and of the Bonn

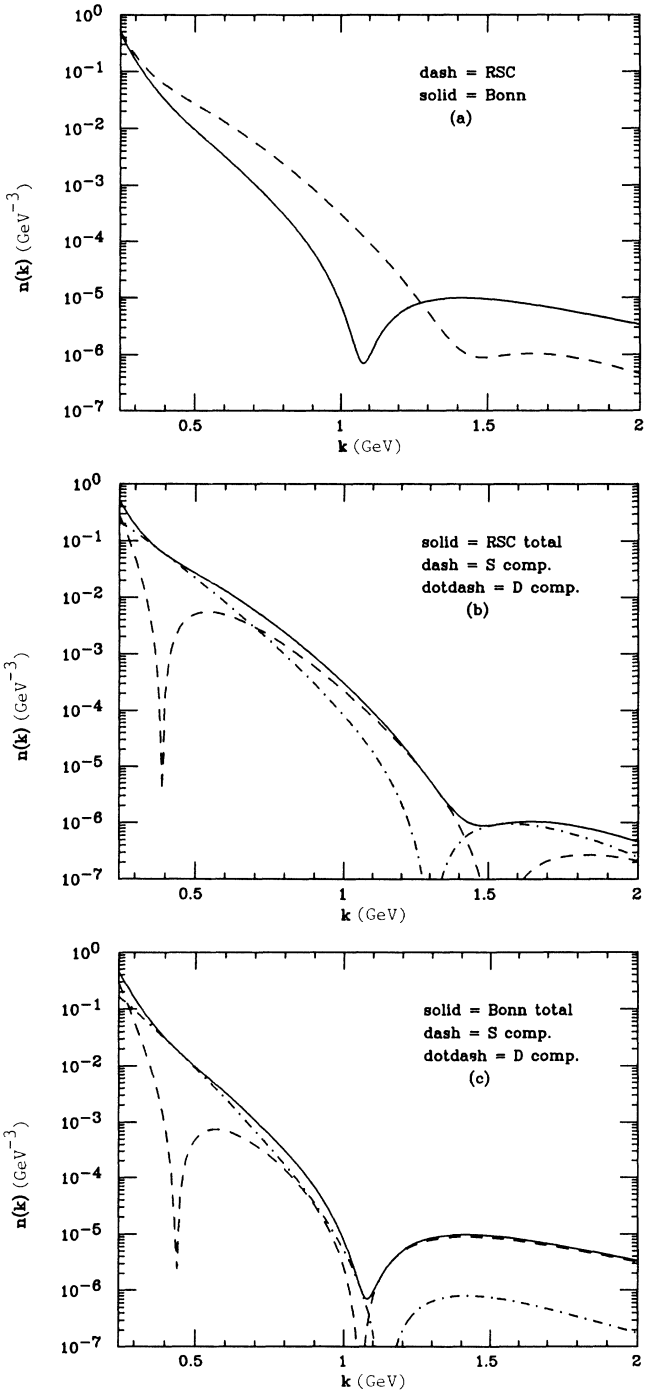

FIG. 1. (a) The total momentum distribution of a single nucleon in a deuterium nucleus for the RSC potential (dashes) and for the Bonn potential (solid). (b) The RSC momentum distribution of a single nucleon in a deuterium nucleus (solid) and its S-state (dashes) and D-state (dotdashes) components. (c) The Bonn momentum distribution of a single nucleon in a deuterium nucleus (solid) and its S-state (dashes) and D-state (dotdashes) components.

N-N potentials. Figure 1(a) presents the total $n(k)$ which is the sum of the S-state (u) and D-state (w) contributions. That is,

$$n(k)=\tilde{u}^{\,2}(k)+\tilde{w}^{\,2}(k)$$

$$=\frac{1}{2\pi^2}\left[\left|\int j_0(kr)u(r)r\,dr\right|^2 + \left|\int j_2(kr)w(r)r\,dr\right|^2\right] . \quad (20)$$

For convenience we use the simplified parametrizations of the deuterium ground-state wave functions as in Refs. 2 and 3. Noticeable differences between the RSC and Bonn distributions are found for $k \gtrsim 0.25$ GeV. RSC is larger than Bonn by more than a factor of 30 at $k=1$ GeV. In the range $1.4 \leq k \leq 2.0$ GeV Bonn is stronger than RSC by about an order of magnitude. Figures 1(b) and 1(c) are intended to elucidate the origins of these differences by displaying separately the S-state and D-state contributions to the total distribution in the RSC and Bonn, respectively. Although the D state constitutes only 6.48% of the RSC ground state and only 4.25% of Bonn ground state, the S-state and D-state contributions to the total momentum distributions are comparable around $k=0.25$ GeV for both potentials. For $0.25 \lesssim k \lesssim 0.60$ GeV the D-state contribution dominates in both cases. For $0.60 \lesssim k \lesssim 1.0$ GeV the situation is more complex. In the case of Bonn the S- and D-state contributions are comparable. On the other hand, for RSC, the S-state contribution is rising relative to the D-state contribution. The net result is that the RSC S-state contribution at $k=1$ GeV is nearly 100 times the S-state contribution from Bonn. On the other hand, the RSC D-state contribution at $k=1$ GeV is only about 20 times the D-state contribution from Bonn. However, when $k \gtrsim 1.3$ GeV the trend reverses; the total from Bonn dominates that from RSC as shown in Fig. 1(a). The data we address are primarily sensitive to these details for k values up to about 0.75 GeV. One main point we wish to stress is that due to the importance of the D state for momenta up to at least 1 GeV one must go beyond this momentum to isolate the role of short-range correlations. This is consistent with a naive picture based on the de Broglie relation where a momentum less than 1 GeV implies distance sensitivity greater than 1 fm. Thus, a major focus of our investigation is upon the intermediate momenta components of deuterium which are dominated by tensor correlations.

The choice of nucleon form factor as a function of Q^2 is a nontrivial issue at the large values of Q^2 with which we are concerned. We will not present an in-depth discussion here but simply select the parametrization of Ref. 12 for $\sigma_p(Q^2)$ and for $\sigma_n(Q^2)$. A detailed comparison among a wide range of choices has been presented and discussed in reference to the nucleon elastic form factor data by Gari and Krümpelmann.[12]

III. THE THREE-QUARK CLUSTERS

In this section we would like to focus on the smearing correction to the inelastic lepton scattering amplitude due to the bound nucleons undergoing Fermi motion in the deuteron. Although there is a controversy[13–16] about how the smearing procedure is implemented there is no doubt that in a nucleon based picture of the nucleus there is a need for treating the Fermi motion.[16] Since the deuteron is not only the simplest but also a diffuse and barely bound nuclear system, one does not intuitively expect the total DIS cross section of the deuteron (σ_d) to be significantly different from the sum of the DIS cross sections of the free nucleons ($\sigma_p+\sigma_n$) in the region where the energy scale is many GeV. However, West[13,14] pointed out that the effect of smearing due to Fermi motion is not negligible.

The assumptions listed below are commonly made for the spin-averaged cross section which we evaluate here. These assumptions are parallel to those made in evaluating the quasielastic process in the preceding section.

(1) The deuteron is considered as a (p,n) bound state in which we neglect the isobar admixture, the six-quark degree of freedom, and the meson exchange current contribution. Later in this paper we consider a specific model, the quark cluster model, for the six-quark effects.

(2) The "off-shell kinematics"–"on-shell dynamics" formalism is adopted. In other words, we use the on-shell amplitude but off-shell kinematics.

(3) We work in the impulse approximation and therefore do not consider the shadowing corrections or final-state interactions (FSI).

Before introducing the smearing procedure, we briefly explain how we have selected the on-shell amplitude squared, the nucleon inelastic structure functions. There exist several parametrizations[17,18]—among them the Buras and Gaemers' (BG) parametrization[17] is widely used. When we compared the results from calculations based on these models with the SLAC proton data (2.5 GeV$^2 \leq Q^2 \leq$ 10.0 GeV^2), we found substantial disagreement since the data exhibit hadronic resonances not accounted for in the models. These parametrizations are typically intended for applications at higher values of Q^2. Therefore we turned to the SLAC parametrization[6] of these same proton data (Fig. 2) which yields a χ^2/data$=2.6$. The quality of this parametrization is clearly seen in contrast to the global (resonance free) fit of BG. This is especially important since much of the deuteron data[5–7] we analyze were taken with these same virtual photon kinematics.

In order to incorporate these resonance effects into the neutron structure function we multiply the SLAC proton structure function by the ratio of the neutron to the proton structure functions in the BG parametrization,

$$\nu W_2^{\mathrm{SLAC}(n)}=\nu W_2^{\mathrm{SLAC}(p)}(\nu W_2^{\mathrm{BG}(n)}/\nu W_2^{\mathrm{BG}(p)}) .$$

Note that since the data we analyze were taken at small laboratory angles (8° and 10°), the W_1 contributions to the cross sections are negligible.

With these assumptions and neglecting the role of spin,

the forward virtual Compton amplitude (Fig. 3) is given as

$$|\mathcal{M}_d(s)|^2=\sum_{i=p,n}\int\frac{d^4k}{(2\pi)^4}\frac{2\pi\phi^2(p^2)\delta(k^2-m^2)}{(p^2-m^2+i\epsilon)^2}\times|\mathcal{M}_i(s')|^2\theta(s'-m^2)$$
$$=\sum_{i=p,n}\int\frac{d^3k}{k_0/m}2|f(\mathbf{k})|^2|\mathcal{M}_i(s')|^2\theta(s'-m^2)\ , \tag{21}$$

where

$$s=(\mathcal{P}+q)^2\ , \tag{22}$$

$$s'=(p+q)^2\ , \tag{23}$$

and

$$|f(\mathbf{k})|^2=\frac{1}{4m(2\pi)^3}\frac{\phi^2(p^2)}{(p^2-m^2+i\epsilon)^2}\ . \tag{24}$$

Now the question is how to recognize the nonrelativistic wave function in Eq. (21). Atwood and West[13,14,16] chose the following normalization:

$$\int\frac{d^3k}{k_0/m}|f(\mathbf{k})|^2=1\ , \tag{25}$$

by identifying $n(k)$, the absolute square of the nonrelativistic deuteron wave function, with $|f(\mathbf{k})|^2/(k_0/m)$. We, however, follow Kusno and Moravcsik,[16] as well as Frankfurt and Strikman,[15] who adopted a different normalization using arguments we summarize below:

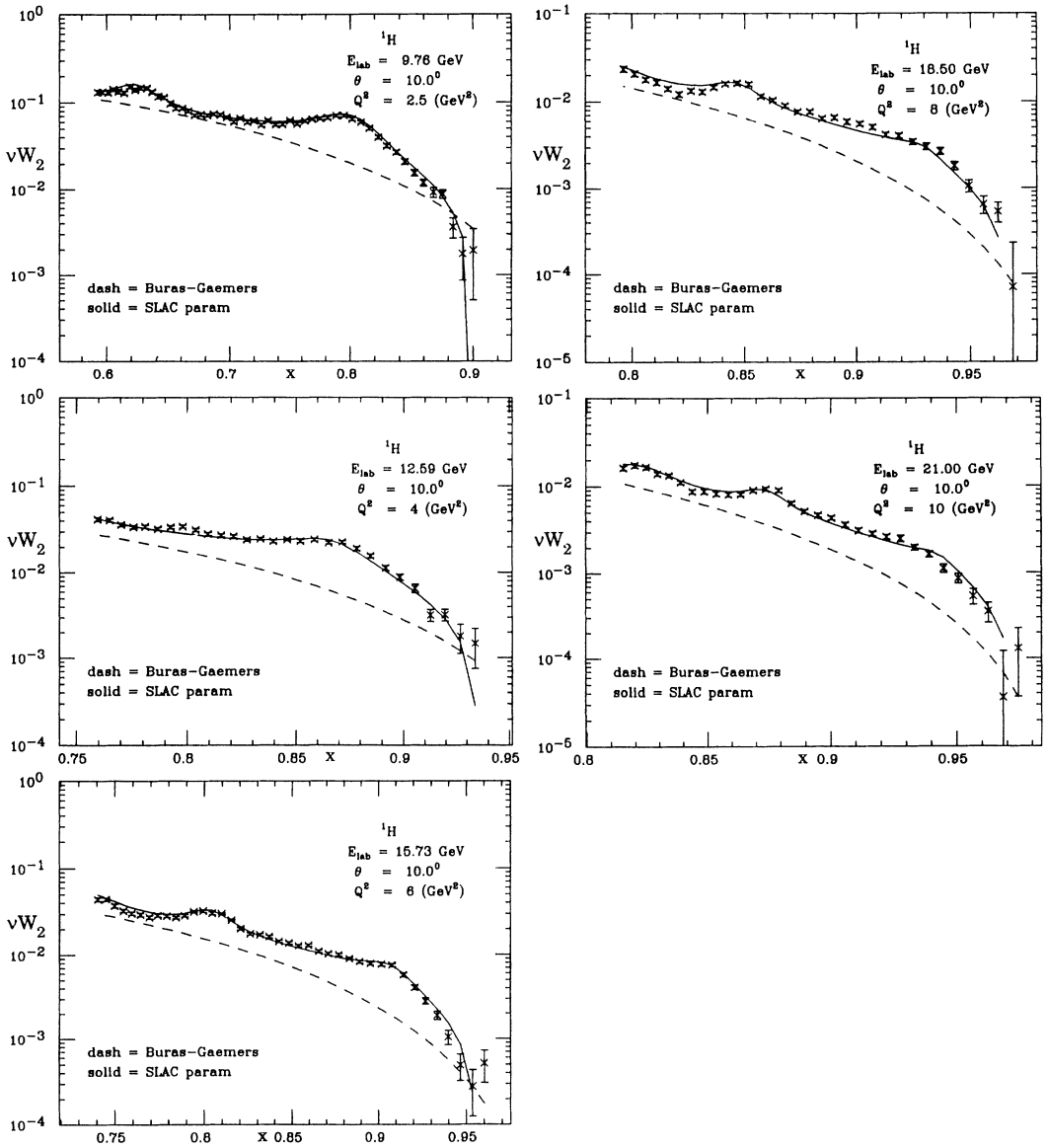

FIG. 2. Electron-proton inclusive data from SLAC experiment E133 (Ref. 6) expressed as νW_2 vs Bjorken x. The solid curve represents the SLAC parametrization discussed in the text while the dashed curve gives the results from the parametrization of Ref. 17.

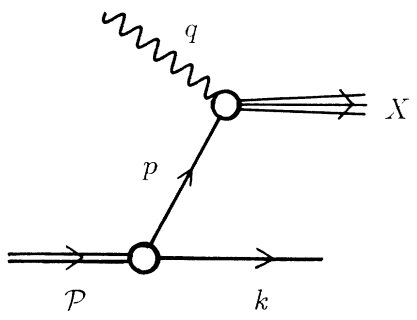

FIG. 3. Impulse-approximation Feynman diagram for the inclusive lepton-deuteron scattering. The wavy line represents the incident virtual photon of four-momentum q; the single solid lines are the struck nucleon of four-momentum p and the spectator nucleon of four-momentum k. The double line represents the target of four-momentum $\mathcal{P}$.

$$\int \frac{d^3k}{k_0/m}|f(\mathbf{k})|^2\frac{2[E_1(|\mathbf{k}|)+k_3]}{M_d}\theta(E_1(|\mathbf{k}|)+k_3)=1\ , \tag{26a}$$

so that we identify

$$n(k)=\frac{m}{k_0}|f(\mathbf{k})|^2\frac{2(E_1(|\mathbf{k}|)+k_3)}{M_d}\ . \tag{26b}$$

Frankfurt and Strikman[15,16] criticized the normalization of Eq. (25) since it is inconsistent with the usual normalization dictated by requiring that the elastic electromagnetic form factor at $Q^2=0$ be equal to the total charge. In addition, Kusno and Moravcsik derived the normalization of Eq. (26a) by using light-front kinematics in Ref. 16 and showed it satisfied the Frankfurt and Strikman criterion. By comparing the normalization of the nonrelativistic wave function we adopted [Eq. (20)] with Eqs. (26), we observe that they agree provided we ignore the θ function in Eq. (26a). Putting in the θ function introduces an error of one part in 10000. Thus our normalization has this error since we retain the θ function throughout our work. Another parametrization of the nucleon momentum density in terms of the light cone variables is $G(x,\mathbf{k}_\perp)$ and is normalized

$$\int d^2k_\perp\int_0^1 dx\ G(x,\mathbf{k}_\perp)=1\ , \tag{27}$$

where x is the light cone fraction on one of the nucleons and $\mathbf{k}_\perp$ is the transverse momentum. The four momenta are defined by

$$\begin{aligned}
\mathcal{P}^\mu&=\left[P+\frac{M_d^2}{4P},\mathbf{0}_\perp,P-\frac{M_d^2}{4P}\right]\ ,\\
q^\mu&=\left[\frac{\mathcal{P}\cdot q}{2P},\mathbf{q}_\perp,-\frac{\mathcal{P}\cdot q}{2P}\right]\ ,\\
k^\mu&=\left[(1-x)P+\frac{k^2+\mathbf{k}_\perp^2}{4(1-x)P},-\mathbf{k}_\perp,(1-x)P-\frac{k^2+\mathbf{k}_\perp^2}{4(1-x)P}\right]\ ,\\
p^\mu&=\left[xP+\frac{(1-x)M_d^2-k^2-\mathbf{k}_\perp^2}{4(1-x)P},\mathbf{k}_\perp,xP-\frac{(1-x)M_d^2-k^2-\mathbf{k}_\perp^2}{4(1-x)P}\right]\ .
\end{aligned} \tag{28}$$

Here $P=\frac{1}{2}(\mathcal{P}_0+\mathcal{P}_3)$ is an arbitrary parameter, and $x=1-(k_0+k_3)/2P$. In the deuteron rest frame $P=\frac{1}{2}M_d$, and $x=1-(k_0+k_3)/M_d$. Meanwhile the function $G(x,\mathbf{k}_\perp)$ is the new function for the integrand of Eq. (26) with the new variables.

Furthermore, we identify the function $G(x,\mathbf{k}_\perp)$ in our notation as

$$G(x,\mathbf{k}_\perp)=\left[M_d+\frac{E_\perp^2}{(1-x)^2M_d}\right]n(\mathbf{k}(x,\mathbf{k}_\perp))\theta(M_d-E_\perp)\ , \tag{29}$$

where $E_\perp=(m^2+\mathbf{k}_\perp^2)^{1/2}$. Therefore, the deuteron inelastic structure obtained through this smearing[16] of the nucleon's (3-q) inelastic structure function over the motion given by $n(\mathbf{k})$ is

$$\nu W_2^{3\text{-}q}(Q^2,\nu)=\sum_{\iota=p,n}\int d^2k_\perp\int_0^1\frac{dx}{x}G(x,\mathbf{k}_\perp)B\frac{\nu}{\nu'}[\nu' W_2^{(\iota)}(Q^2,\nu')]\ , \tag{30}$$

where $\nu'=(p\cdot q)/2m$ is different from $\nu=(\mathcal{P}\cdot q)/2m$, and

$$B=\frac{1}{2(q^2M_d^2-m^2\nu^2)^2}\{2x^2m^4\nu^4-4xm^3\nu^3(\mathbf{q}_\perp\cdot\mathbf{k}_\perp)+m^2\nu^2[q^2C_3+2(\mathbf{q}_\perp\cdot\mathbf{k}_\perp)^2]+m\nu q^2(\mathbf{q}_\perp\cdot\mathbf{k}_\perp)C_4+q^4C_5+q^2M_d^2(\mathbf{q}_\perp\cdot\mathbf{k}_\perp)^2\}\ , \tag{31}$$

and where

$$C_3=\frac{1}{1-x}[2xm^2-2x(1-x^2)M_d^2+(3x-1)\mathbf{k}_\perp^2]\ ,$$

$$C_4=\frac{1}{1-x}\{-3E_\perp^2+[4-(1+x)^2]M_d^2\}\ ,$$

$$C_5=\frac{3\mathbf{k}_\perp^4}{4(1-x)^2}+\frac{\mathbf{k}_\perp^2}{2(1-x)^2}[3m^2+(3x^2-2x-1)M_d^2]$$
$$+\frac{1}{4(1-x)^2}[3m^4+2m^2M_d^2(x^2+2x-3)+M_d^4(3x^4-4x^3+2x^2-4x+3)]\ . \quad (32)$$

IV. RESULTS FROM THE "CONVENTIONAL" APPROACH

As discussed in Sec. II the quasielastic single nucleon knockout mechanism contributes significantly to the inelastic cross section in the kinematic range within which the deuteron data were taken—Q^2 between 2.5 and 10 GeV^2; the quasielastic peak is clearly revealed in the data. In order to describe the data, therefore, the deuteron inelastic structure function at least should contain the incoherent sum of the quasielastic $\nu W_2^{\rm qel}$ (Sec. II) and the smeared inelastic structure functions (Sec. III). That is,

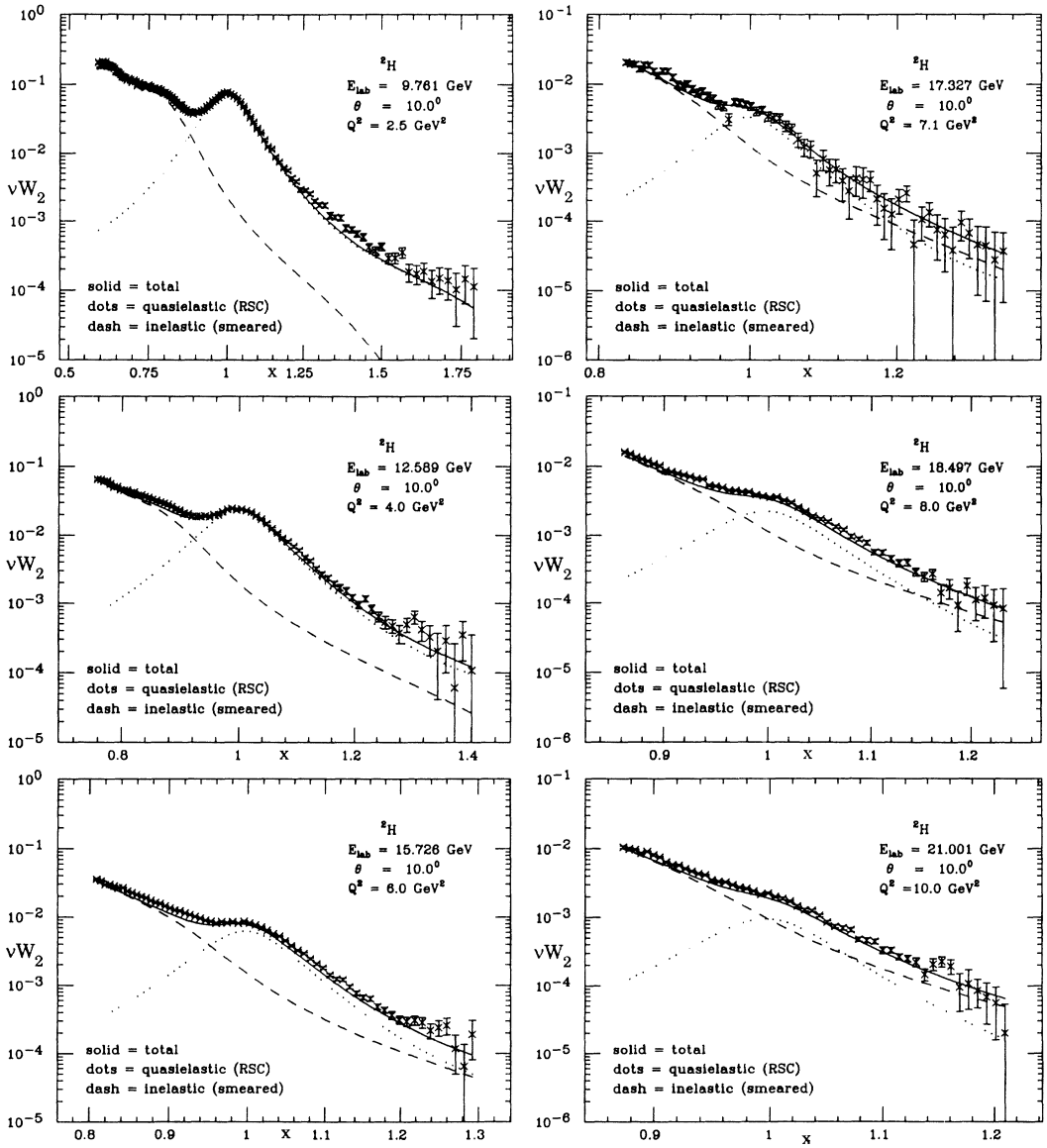

FIG. 4. Electron-deuteron inclusive data from SLAC experiment E133 (Ref. 6) expressed as νW_2 vs Bjorken x compared with the conventional approach based on the RSC wave function. The quasielastic component is represented by the dotted curve and the 3-q smeared inelastic is represented by the dashed curve. The solid curve represents the incoherent sum of these contributions.

$$\nu W_2^{(D)} = \nu W_2^{\text{qel}} + \nu W_2^{3\text{-q}} \ . \tag{33}$$

We refer to $\nu W_2^{(D)}$ given by Eq. (33) as the "conventional" approach since it relies in a major way on measured free-space elastic and inelastic properties of nucleons and on traditional models of nuclear structure.

Utilizing this approach we present comparisons with data in Figs. 4, 5, 6, and 7 for selected data sets[5–7] in the range $2.5 \lesssim Q^2 \lesssim 10.0$ GeV^2. The results are plotted as a function of Bjorken $x = Q^2/2m\nu$ for $\nu W_2^{(D)}$ which, for the data, is *defined* as the double-differential cross section multiplied by ν and divided by the Mott cross section σ_M. The results of Figs. 4 and 6 correspond to the RSC (Ref. 2) potential while those of Figs. 5 and 7 correspond to the Bonn[3] potential. The calculations are performed in the following two ways. First, all the values of νW_2 are calculated at a fixed Q^2 and θ (8° or 10°), with ν and E (or E') changing to cover the desired range of x. Second, the calculations are performed at the Q^2, ν values corresponding to each data point and joined by a smooth curve. These two methods lead to indistinguishable theoretical results.

The first major impression gained from Figs. 4–7 is that for the values of $x > 1$ there is a substantial contribution from quasielastic knockout evaluated with conventional nuclear models in lowest order (i.e., with the neglect of final-state interactions). This conclusion is true for calculations based on RSC and on Bonn wave functions. We do not concentrate here on the discrepancies between theory and data which will be resolved in a later

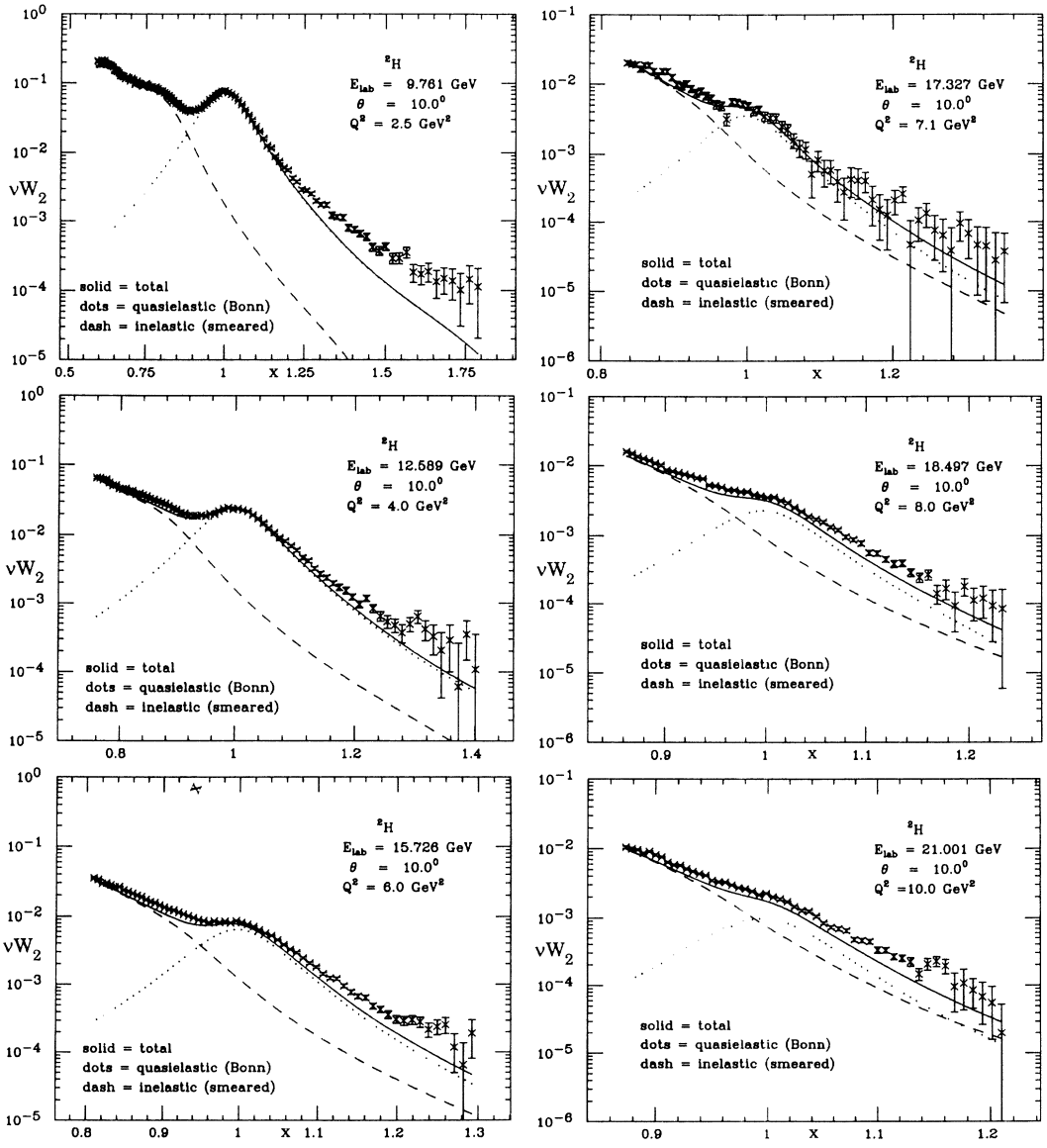

FIG. 5. Electron-deuteron inclusive data from SLAC experiment E133 (Ref. 6) expressed as νW_2 vs Bjorken x compared with the conventional approach based on the Bonn wave function. The quasielastic component is represented by the dotted curve and the 3-q smeared inelastic is represented by the dashed curve. The solid curve represents the incoherent sum of these contributions.

section. The second major conclusion concerns the region $x < 1$ where we find large contributions from the nucleon inelastic structure function. These inelastic contributions show approximate Bjorken scaling (independence of Q^2 at fixed x) and hence become more important with increasing Q^2 relative to the quasielastic nucleon knockout process. This is clearly seen in the data for νW_2 where there is approximate independence of Q^2 at $x = 0.75$ whereas the data at the quasielastic peak ($x = 1$) decrease by about a factor of 44 as Q^2 increases from 2.5 to 10.0 GeV^2. Indeed the behavior of the quasielastic peak and the entire $x > 1$ data have been extensively studied in terms of y scaling.[7,9] The calculated curves are instructive since the total result follows the trends in the data and since the quasielastic component reflects pure y scaling while the inelastic component nearly exhibits Bjorken x scaling. The trend in the calculated curves from $Q^2 = 2.5$ to 10.0 GeV^2 indicates the data are approaching a region where Bjorken scaling should set in and, hence, y scaling should become invalid. The onset of x scaling for $x > 1$ is about the same for the results obtained with both the RSC and the Bonn wave functions.

The sensitivity to the deuteron wave function for $x > 1.25$ is clearly seen by comparing the results in Figs. 4–7. The Bonn wave function significantly underpredicts the data while the RSC does reasonably well in this kinematic region. We have examined the individual S-state and D-state contributions to $\nu W_2^{\rm qel}$ and have found that,

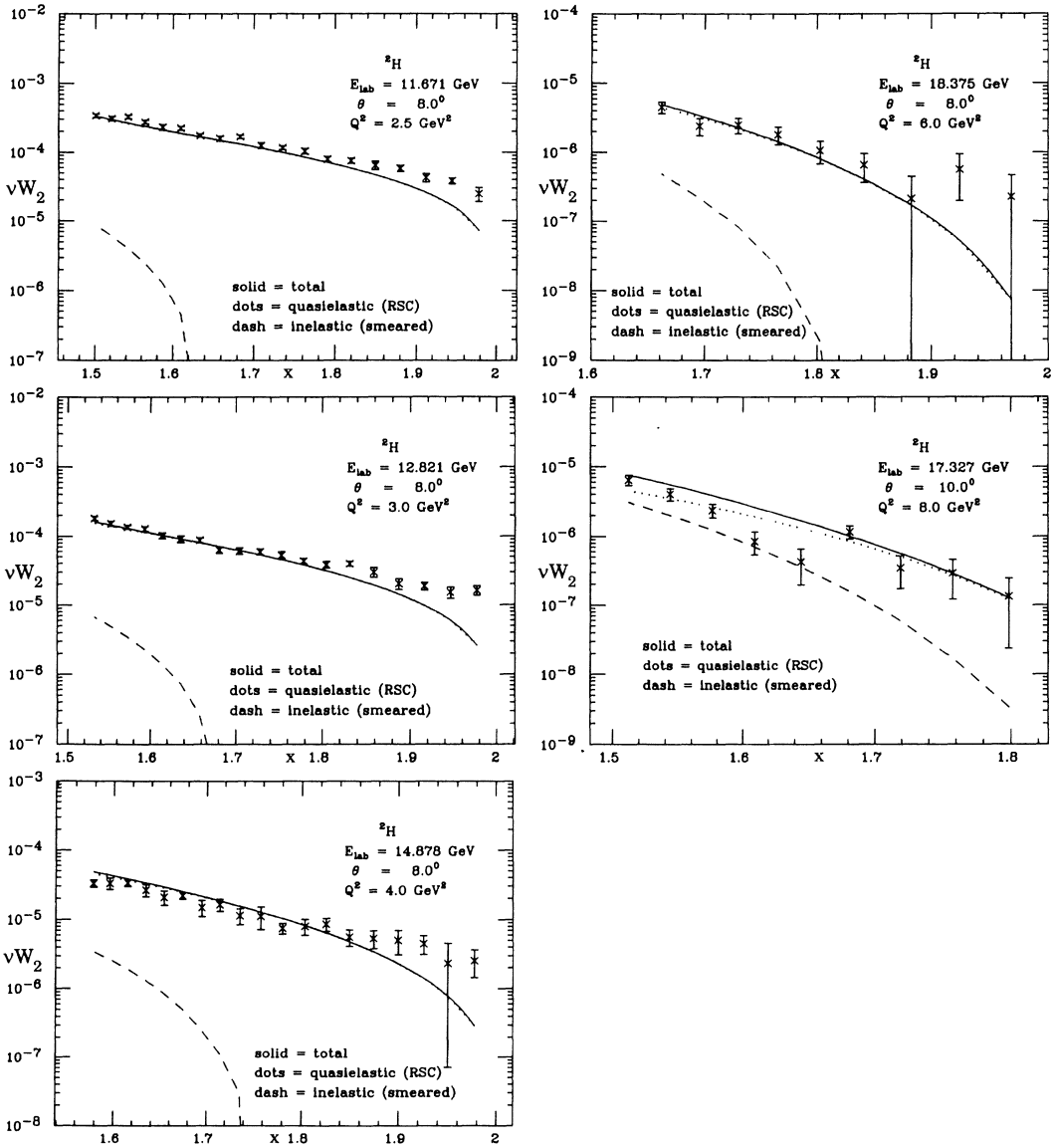

FIG. 6. Electron-deuteron inclusive data from SLAC experiment E101 (Ref. 5) expressed as νW_2 vs Bjorken x compared with the conventional approach based on the RSC wave function. The quasielastic component is represented by the dotted curve and the 3-q smeared inelastic is represented by the dashed curve. The solid curve represents the incoherent sum of these contributions.

in all cases shown, it is the D-state contribution which dominates for $1.25 \leq x \leq 1.75$. For $x > 1.75$ the S-state contribution again becomes significant. The better agreement obtained with RSC is due to its enhanced momentum components in the range $0.25 \lesssim k \lesssim 1.0$ GeV which were described above.

Some recent efforts[19] have obtained results for low-energy properties of nuclei which may favor the Bonn potential over the RSC potential. Up to this stage our applications in this paper would tend to favor the RSC results over the Bonn results. However, we feel our results should not be viewed as providing a definitive test of these wave functions. Rather, additional effects, such as the six-quark cluster effects evaluated below, should be included with a representative sample of realistic wave functions in order to obtain a true perspective of their potential significance.

A significant uncertainty in the overall magnitude of our results for $\nu W_2^{\rm qel}$ in Figs. 4–7 arises from uncertainties in the nucleon elastic form factors. The detailed studies by Gari and Krümpelmann[12] indicate that these uncertainties increase substantially for $Q^2 > 4$ GeV^2. It is satisfying that the quasielastic peak in conjunction with $\nu W_2^{3\text{-q}}$ reasonably tracks with Q^2 the measured νW_2 at $x = 1$. Some improvement of the agreement between the conventional approach and the data may be achieved by modifying the nucleon form factors but we have not elected to explore that challenging problem in the current work.

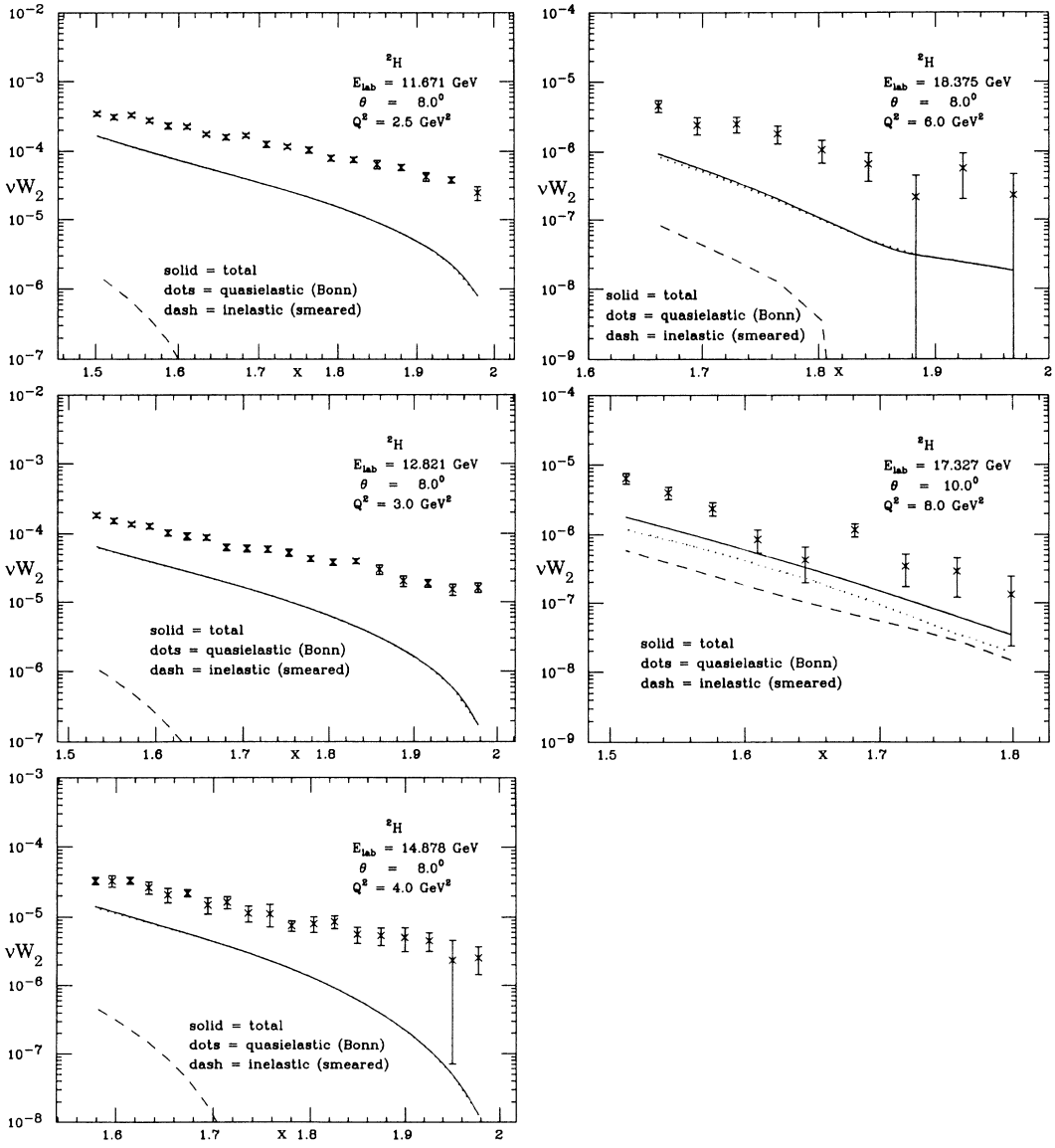

FIG. 7. Electron-deuteron inclusive data from SLAC experiment E101 (Ref. 5) expressed as νW_2 vs Bjorken x compared with the conventional approach based on the Bonn wave function. The quasielastic component is represented by the dotted curve and the 3-q smeared inelastic is represented by the dashed curve. The solid curve represents the incoherent sum of these contributions.

V. THE QUARK CLUSTER MODEL

As shown in the figures in the preceding section, in the high x region, especially with higher Q^2 there is still room for improvement in the model to obtain better agreement with the data. We, therefore, introduce the six-quark (6-q) cluster component of the quark cluster model[4] (QCM) into our calculation in this section. The QCM was first introduced to fit certain $x>1$ features of the ^{3}He DIS data.[20] A careful analysis based on the conventional nuclear physics[21] (only nucleonic degree of freedom considered) had been unsuccessful. Later, it was shown[22] that the QCM is also capable of explaining the European Muon Collaboration (EMC) effect.[23] There are three main assumptions of the QCM. The first two are traditional assumptions for any parton model interpretation of deep-inelastic lepton-hadron data while the third is particular to the nuclear environment. The assumptions of the QCM are as follows.

(1) A photon absorbed by a nucleus at high Q^2 is absorbed by a quark through a quasifree process when viewed in the infinite momentum frame.

(2) The quark is a constituent of a quasifree color-singlet cluster in the nucleus.

(3) A three-quark (3-q) cluster (nucleon) is assigned a critical radius R_C. Clusters with $i=6,9,12,\ldots,3A$ quarks are defined by the number of 3-q clusters joined by links of length $\leq 2R_C$.

The critical radius R_C is taken as a free parameter and adjusted to fit data. If $R_C=0$ gives the best overall fit to the data, then no quark clusters other than nucleons (3-q) are formed, and the conventional approach presented in the preceding sections survives. On the other hand, if R_C is large, say 1.5 fm, the nucleus has a high probability of being found in the 3A-q cluster configuration. R_C was found to be 0.50 ± 0.05 fm from fitting the ^{3}He data. In what follows we show that $R_C=0.50$ fm yields a 4.7% (5.4%) 6-q cluster configuration in deuterium with the RSC (Bonn) wave function and we examine the consequences for the description of the DIS deuterium data.

The model is easily visualized in the Breit frame defined by requiring the quark which absorbs the photon to have longitudinal momentum $+k$ before and $-k$ after the interaction. Therefore, the four-momentum of the virtual photon in this frame is $q^\mu=(0,\mathbf{0}_\perp,-2k)$, and $Q^2=4k^2$. If the initial target four-momentum is $P^\mu=(E_P,\mathbf{0}_\perp,P)$ in the same frame, then

$$2P^\mu q_\mu=2P(-2k)=-2Am\nu \ . \tag{34}$$

As a result

$$k=\frac{x}{A}P \ , \tag{35}$$

with $x=Q^2/2m\nu$. Thus, x/A is the fraction of the total nuclear momentum P carried by the struck quark. The inelastic nuclear structure function hence can be written, according to the parton model, as

$$\nu W_2(\nu,Q^2)=\sum_{\text{quarks } j} e_j^2\frac{x}{A}\mathcal{N}_j(x) \ , \tag{36}$$

where we sum over all quarks in the nucleus, e_j is the charge on the quark j, and $\mathcal{N}_j(x)$ is the probability of finding quark j carrying fraction x/A of the total nuclear momentum P. If we approximate with a properly weighted average of up and down quark distributions, $\mathcal{N}(x)$, we can write

$$\nu W_2(\nu,Q^2)\simeq\sum_{\text{quarks } j} e_j^2\frac{x}{A}\mathcal{N}(x) \ . \tag{37}$$

According to the model assumptions[4] the quarks are found in an i-quark cluster ($i=3,6,\ldots,3A$) within the nucleus with probability $\bar{p}_i$ so that

$$\mathcal{N}(x)=\sum_{\text{clusters } i}\bar{p}_i\bar{P}_i(x) \ , \tag{38}$$

where $\bar{P}_i(x)$ is the x distribution of quarks from an i-q cluster in the nucleus. Therefore, if we write

$$\nu W_2^{3\text{-q}}=\sum_{j=1}^{3}e_j^2\frac{x}{A}\bar{P}_3(x) \ , \tag{39}$$

$$\nu W_2^{6\text{-q}}=\sum_{j=1}^{6}e_j^2\frac{x}{A}\bar{P}_6(x) \ , \tag{40}$$

then the deuteron inelastic structure function is written as

$$\nu W_2^{(D)}=\tilde{p}_3(\nu W_2^{3\text{-q}}+\nu W_2^{\text{qel}})+\tilde{p}_6(\nu W_2^{6\text{-q}}) \ , \tag{41}$$

where

$$\tilde{p}_3=\int_{2R_C}^{\infty}dr[u^2(r)+w^2(r)] \ , \tag{42}$$

$$\tilde{p}_6=\int_{0}^{2R_C}dr[u^2(r)+w^2(r)] \ , \tag{43}$$

with $\tilde{p}_3+\tilde{p}_6=1$. We carry out these integrals with $R_C=0.50$ fm for both the RSC and Bonn wave functions. We obtain $\tilde{p}_3=0.953$ and $\tilde{p}_6=0.047$ for RSC and $\tilde{p}_3=0.946$ and $\tilde{p}_6=0.054$ for Bonn. The larger 6-q cluster probability for Bonn reflects somewhat weaker short-range correlations.

The above description has been qualitative in that it neglects the role of transverse motion. The more complete description of Sec. III will be adopted for $\nu W_2^{3-\text{q}}$. Since the 6-q cluster is at rest in the nuclear c.m. frame for deuterium there is no need to consider its transverse motion. Therefore, the "6-q structure function," $\nu W_2^{6-\text{q}}$, with the modification of replacing x by ξ, the Nachtmann quark variable,[24] is argued[4,22] to be

$$\nu W_2^{6\text{-q}}=\frac{\xi}{2}\left[\sum_{i=1}^{6}e_i^2\right]\bar{P}_6(\xi) \ , \tag{44}$$

where

$$\bar{P}_6(\xi)=\frac{1.850\,069}{\sqrt{\xi/2}}\left[1-\frac{\xi}{2}\right]^{10} \ , \tag{45}$$

with

$$\xi=\frac{2x}{1+(1+Q^2/\nu^2)^{1/2}} \ . \tag{46}$$

Much of the $x\sim 2$ data we study were acquired with

the final-state invariant mass only a few tens of MeV above breakup threshold. The 6-q inelastic structure function should be modified to respect at least the phase-space limitations just above this threshold.[25] We therefore introduce a threshold factor $\mathcal{R}_{\rm ps}$ to modify the 6-q structure function [Eq. (44)]:

$$\nu W_2^{6\text{-q}} = \mathcal{R}_{\rm ps} \frac{\xi}{2} \left[\sum_{i=1}^{6} e_i^2 \right] \bar{P}_6(\xi) , \tag{47}$$

where

$$\mathcal{R}_{\rm ps} = \begin{cases} \sqrt{1-(2m/W)}, & \text{if } W > 2m, \\ 0, & \text{otherwise.} \end{cases} \tag{48}$$

Here $W^2 = s = (\mathcal{P}+q)^2$.

VI. RESULTS WITH THE FULL QUARK CLUSTER MODEL

We proceed to compare the same data sets as above with the results of the full QCM. In Fig. 8 (10) we present the QCM results for the RSC wave function in comparison with the SLAC E133 (E101) data. The 3-q and the 6-q cluster contributions at fixed $x > 1$ clearly rise together with Q^2 relative to the quasielastic contribution. However, excluding the E101 data in Fig. 10 for $Q^2 \geq 6.0$ GeV^2, these inclusive data do not go to sufficiently high x and sufficiently high Q^2 to be sensitive to the 6-q cluster contribution when the model is based on the RSC wave function. For the E101 data at $Q^2 \geq 6.0$ GeV^2 the model calculations show large contributions from the 6-q cluster but the present uncertainties in the data prevent us from

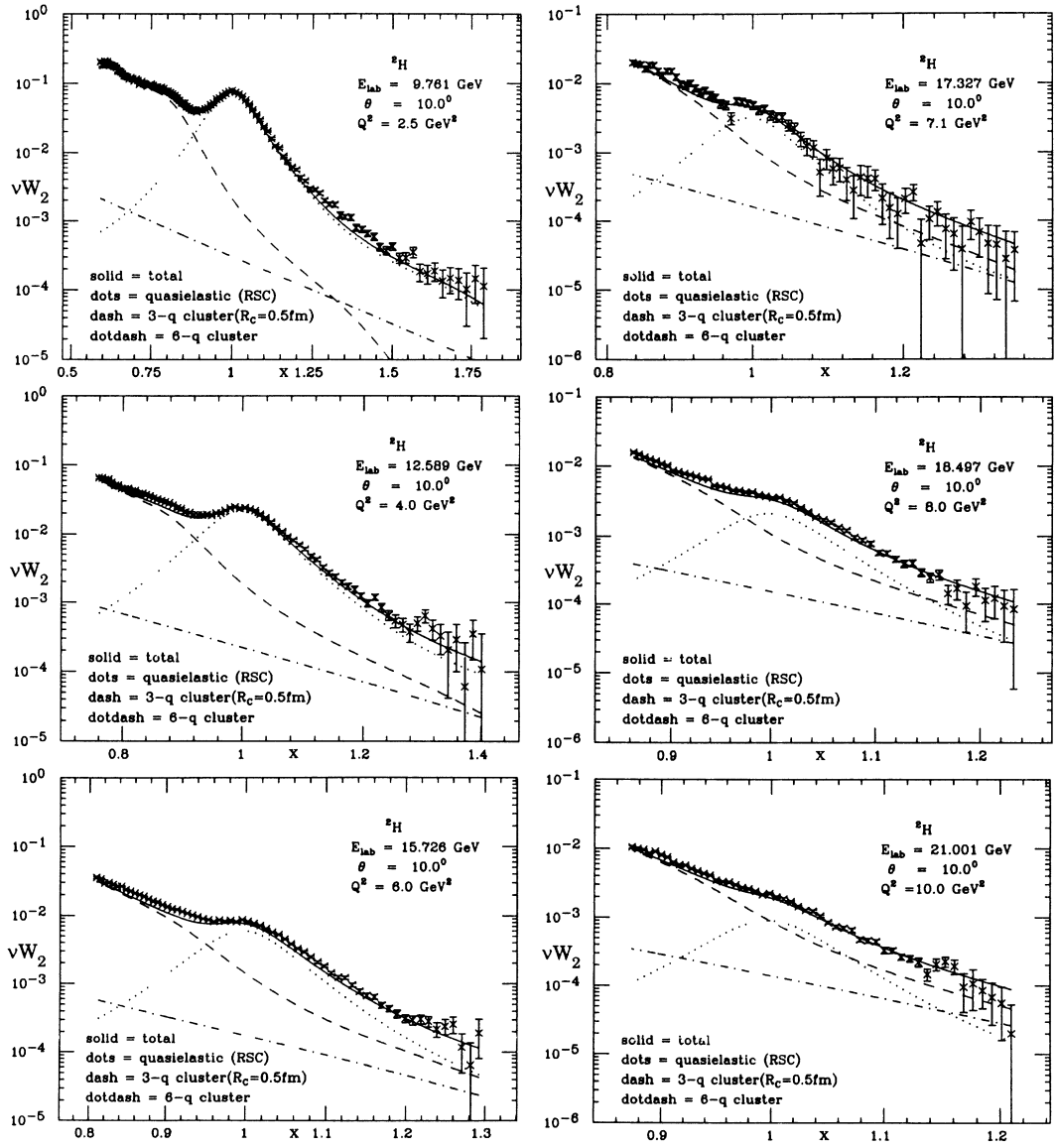

FIG. 8. Electron-deuteron inclusive data from SLAC experiment E133 (Ref. 6) expressed as νW_2 vs Bjorken x compared with the results from the quark cluster model based on the RSC wave function. The quasielastic component is represented by the dotted curve and the 3-q smeared inelastic is represented by the dashed curve. The dot-dashed curve stands for the 6-q inelastic. The solid curve represents the incoherent sum of these contributions.

making definitive conclusions. As a consequence we can say the conventional approach (Figs. 4 and 6) and the QCM (Figs. 8 and 10) when based on the RSC wave function provide an equally acceptable description of these data.

In Figs. 9 and 11 we present the QCM results for the Bonn wave function in comparison with the same data sets. Here, we observe rather dramatic consequences due to the 6-q cluster contributions. The overall agreement between theory and experiment is considerably improved by the QCM in the $x > 1$ region over the conventional results of Figs. 5 and 7.

VII. CONCLUSIONS

We have evaluated the contribution of quasifree nucleon knockout and of inelastic lepton-nucleon scattering in inclusive electron-deuteron reactions at large momentum transfer. We examined the degree of quantitative agreement with deuteron wave functions from the RSC and Bonn realistic nucleon-nucleon interactions. For the range of data available we showed there is strong sensitivity to the tensor correlations which are distinctively different in these two deuteron models. At this stage the RSC wave function provided a reasonable description of

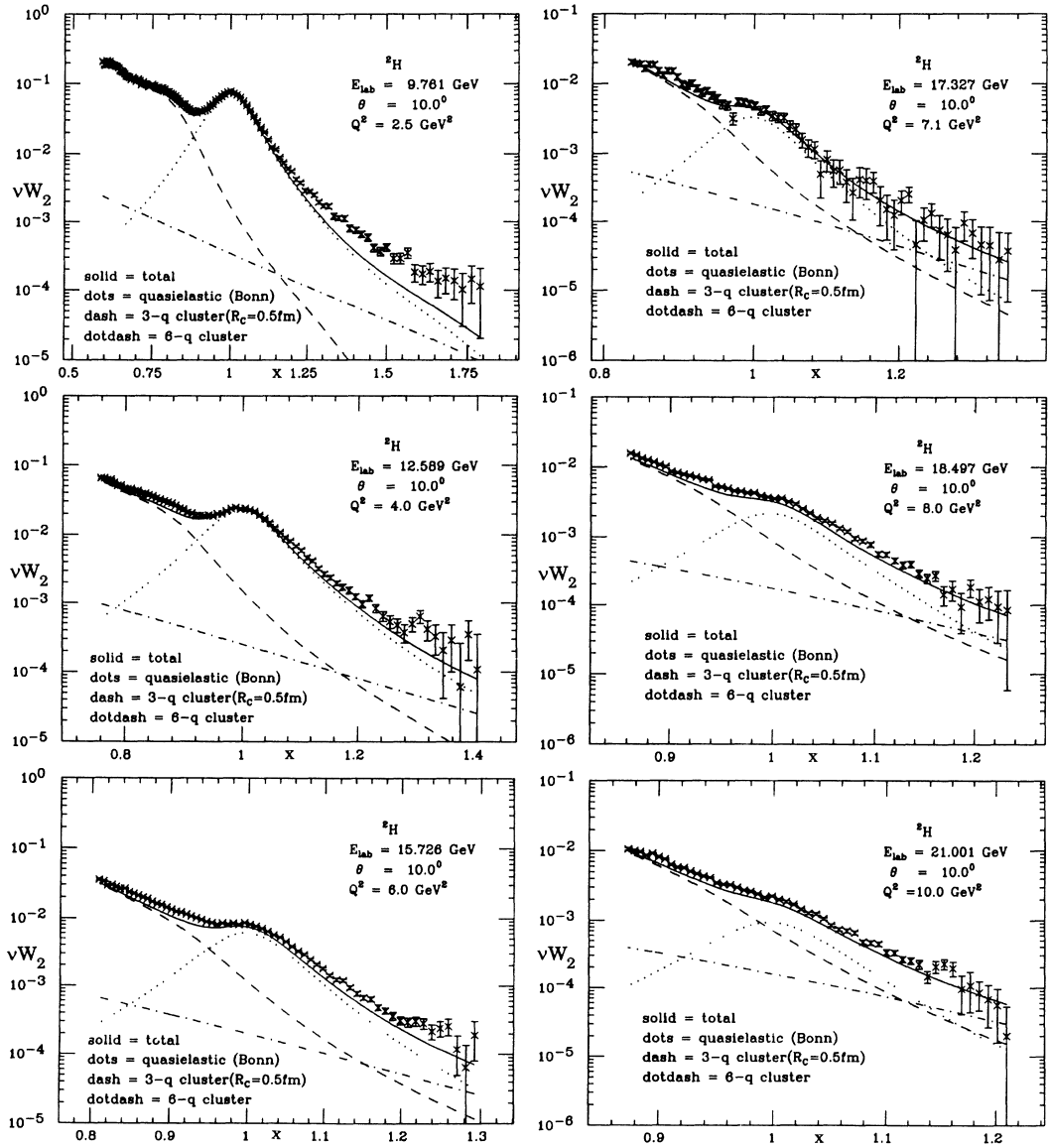

FIG. 9. Electron-deuteron inclusive data from SLAC experiment E133 (Ref. 6) expressed as νW_2 vs Bjorken x compared with the results from the quark cluster model based on the Bonn wave function. The quasielastic component is represented by the dotted curve and the 3-q smeared inelastic is represented by the dashed curve. The dot-dashed curve stands for the 6-q inelastic. The solid curve represents the incoherent sum of these contributions.

the data while the Bonn wave function did not. We then introduced a 6-q cluster component whose relative contribution is based on an overlap criterion and obtained a good description of all the data with both interactions. The critical separation at which overlap occurs (formation of 6-q clusters) is taken to be 1.0 fm and the 6-q cluster probability is 4.7% for RSC and 5.4% for Bonn. It has been speculated that an additional signal of 6-q clusters in these DIS data could be observable through coherent effects between the 3-q and 6-q inelastic contributions.[26]

The description of the DIS deuterium data with the QCM is as good as the conventional description when both are based on the RSC wave function. The description of the same data with the QCM is definitely superior to the conventional description when both are based on the Bonn wave function. The QCM results with the Bonn wave function are similar to the QCM results with RSC even though their respective results in the conventional model were very different. This implies that the QCM is more "robust" (i.e., has greater independence of the adopted deuterium wave function) than the conventional approach. It is easy to see why this is true. For fixed R_C, as one diminishes the short- and intermediate-range correlations the large x contributions from the quasielastic and 3-q inelastic processes decrease. At the same time $\tilde{p}_6$ will increase and therefore larger 6-q cluster contributions will emerge offsetting the decreases in the other processes.

It is worthwhile to recall that there are a number of ap-

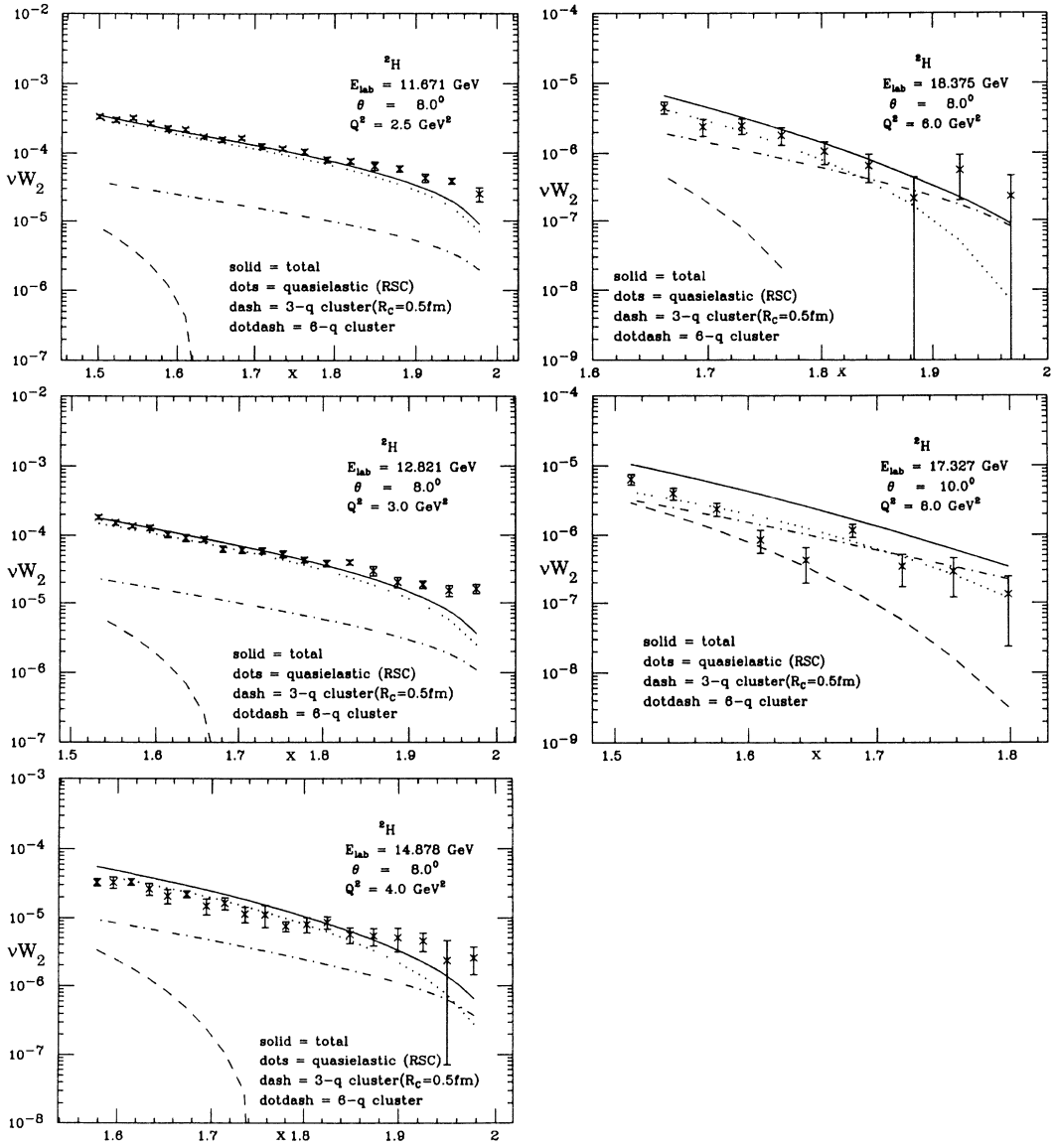

FIG. 10. Electron-deuteron inclusive data from SLAC experiment E101 (Ref. 5) expressed as νW_2 vs Bjorken x compared with the results from the quark cluster model based on the RSC wave function. The quasielastic component is represented by the dotted curve and the 3-q smeared inelastic is represented by the dashed curve. The dot-dashed curve stands for the 6-q inelastic. The solid curve represents the incoherent sum of these contributions.

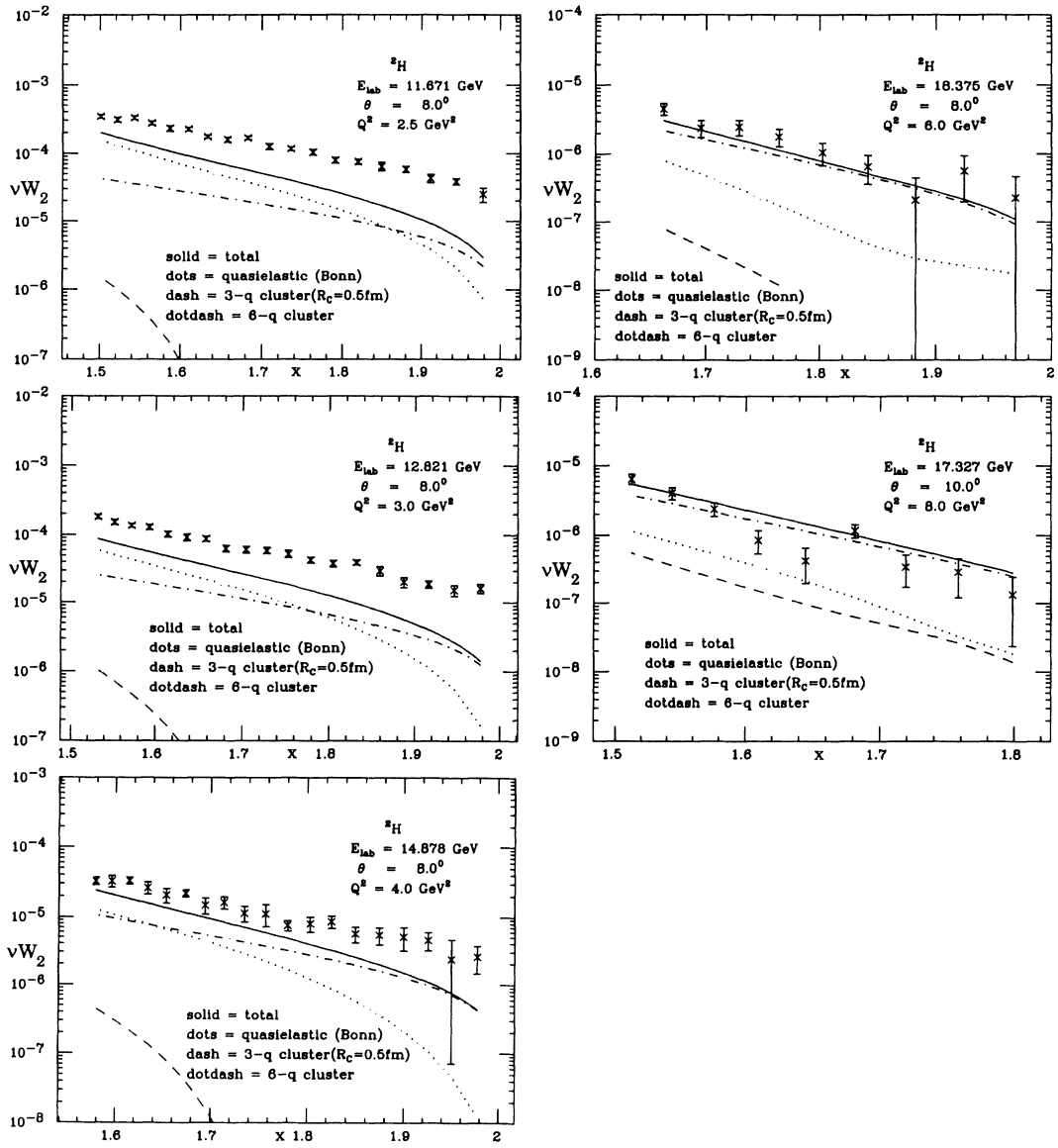

FIG. 11. Electron-deuteron inclusive data from SLAC experiment E101 (Ref. 5) expressed as νW_2 vs Bjorken x compared with the results from the quark cluster model based on the Bonn wave function. The quasielastic component is represented by the dotted curve and the 3-q smeared inelastic is represented by the dashed curve. The dot-dashed curve stands for the 6-q inelastic. The solid curve represents the incoherent sum of these contributions.

proximations made in developing the models presented herein. Two approximations which stand out as limiting the strength of our conclusions are the use of deuteron wave functions from the nonrelativistic formalism and the neglect of final-state interactions. It is hoped that these limitations can be removed in future efforts.

In view of our results it is worth speculating on experiments which could help resolve which wave function forms a superior basis for comparison with data. Inclusive data at $x > 1$ and at higher Q^2 would be one avenue since RSC and Bonn still differ somewhat in that region. More exclusive data, such as $(e,e'\pi)$ for $x > 1$ even at somewhat lower Q^2, could resolve between these models and wave functions since the integrated yield could be compared with the sum of the $\nu W_2^{3\text{-}q}$ and $\nu W_2^{6\text{-}q}$ presented in the various models here. It is our hope that these theoretical results will strongly motivate new experiments in these directions.

ACKNOWLEDGMENTS

We acknowledge useful communications with R. Arnold, P. Bosted, R. Machleidt, and S. E. Rock. This work was supported in part by the U.S. Department of Energy under Contract No. DE-FG02-87ER40371, Division of High Energy and Nuclear Physics.

[1]For a review, see E. L. Berger, *Intersections Between Particle and Nuclear Physics, Lake Louise, Canada, 1986,* in Proceedings of the Second Conference on the Intersections Between Particle and Nuclear Physics, AIP Conf. Proc. No. 150, edited by D. F. Geesaman (AIP, New York, 1986).

[2]R. V. Reid, Ann. Phys. (N.Y.) **50**, 411 (1968); J. M. Greban, private communication.

[3]R. Machleidt, K. Holinde, and Ch. Elster, Phys. Rep. **149**, 1 (1987), and references therein.

[4]H. J. Pirner and J. P. Vary, Phys. Rev. Lett. **46**, 1376 (1981); Nucl. Phys. **A358**, 413c (1981); M. Sato, S. A. Coon, H. J. Pirner, and J. P. Vary, Phys. Rev. C **33**, 1062 (1986).

[5]W. P. Schütz, R. G. Arnold, B. T. Chertok, E. B. Dally, A. Grigorian, C. L. Jordan, and R. Zdarko, Phys. Rev. Lett. **38**, 259 (1977).

[6]S. Rock, R. G. Arnold, P. Bosted, B. T. Chertok, B. A. Mecking, I. Schmidt, Z. M. Szalata, R. C. York, and R. Zdarko, Phys. Rev. Lett. **49**, 1139 (1982); S. Rock, private communcation.

[7]P. Bosted R. G. Arnold, S. Rock, and Z. Szalata, Phys. Rev. Lett. **49**, 1380 (1982).

[8]J. D. Bjorken and S. D. Drell, *Relativistic Quantum Mechanics* (McGraw-Hill, New York, 1964).

[9]G. West, Phys. Rep. **18C**, 265 (1975); I. Sick, Phys. Lett. **157B**, 13 (1985); C. Ciofi degli Atti, E. Pace, and G. Salmè, *ibid.* **127B**, 303 (1983); Phys. Rev. C **36**, 1208 (1987); G. Yen, A. Harindranath, J. P. Vary, and H. J. Pirner, Phys. Lett. B **218**, 408 (1989).

[10]L. S. Celenza, W. S. Pong, M. M. Rahman, and C. M. Shakin, Phys. Rev. C **26**, 320 (1982).

[11]T. de Forest, Nucl. Phys. **A392**, 232 (1983).

[12]M. Gari and W. Krümpelmann, Z. Phys. A **322**, 689 (1985); Phys. Lett. B **173**, 10 (1986).

[13]G. B. West, Phys. Lett. **37B**, 509 (1971); Ann. Phys. (N.Y.) **74**, 464 (1972).

[14]W. B. Atwood and G. B. West, Phys. Rev. D **7**, 773 (1973).

[15]L. L. Frankfurt and M. I. Strikman, Phys. Lett. **64B**, 433 (1976); **65B**, 51 (1976); **76B**, 333 (1978).

[16]D. Kusno and M. J. Moravcsik, Phys. Rev. D **20**, 2734 (1979); Phys. Rev. C **27**, 2173 (1983).

[17]A. J. Buras and K. J. F. Gaemers, Nucl. Phys. **B132**, 249 (1978).

[18]L. F. Abbott, W. B. Atwood, and R. M. Barnett, Phys. Rev. D **22**, 582 (1980); D. W. Duke and J. F. Owens, *ibid.* **30**, 49 (1984).

[19]R. A. Brandenburg, G. S. Chulick, Y. E. Kim, D. J. Klepacki, R. Machleidt, A. Picklesimer, and R. M. Thaler, Phys. Rev. C **37**, 781 (1988).

[20]D. Day, J. S. McCarthy, I. Sick, R. G. Arnold, B. T. Chertok, S. Rock, Z. M. Szalata, F. Martin, B. A. Mecking, and G. Tamas, Phys. Rev. Lett. **43**, 1143 (1979).

[21]H. Meier-Hajduk, Ch. Hajduk, P. U. Sauer, and W. Theis, Nucl. Phys. **A395**, 332 (1983).

[22]C. E. Carlson and T. J. Havens, Phys. Rev. Lett. **51**, 261 (1983).

[23]European Muon Collaboration (EMC), J. J. Aubert *et al.*, Phys. Lett. **123B**, 275 (1983).

[24]O. Nachtmann, Nucl. Phys. **B63**, 237 (1973).

[25]E. Byckling and K. Kajantie, *Particle Kinematics* (Wiley, London, 1973).

[26]G. D. Yen and J. P. Vary, Phys. Rev. C **40**, R16 (1989).